



# Some effects of population interaction on a multi-population SIRC epidemiological model

## Algunos efectos de la interacción poblacional en un modelo epidemiológico SIRC multipoblacional

 Joice Chaves Marques<sup>1</sup> and  Adriano De Cezaro<sup>1</sup>,

---

✉ Joice Chaves Marques: [joicec.marques@hotmail.com](mailto:joicec.marques@hotmail.com)

<sup>1</sup> Instituto de Matemática, Estatística e Física,  
Universidade Federal do Rio Grande  
Rio Grande, Brazil

Recepción: 2023-04-05 | Aceptación: 2023-07-30 | Publicación: 2023-10-29

**Recommended Citation:** Chaves Marques, J *et al.* (2023). 'Some effects of population interaction on a multi-population SIRC epidemiological model'. Rev. model. mat. sist. biol. 3(E), e23E01, doi:10.58560/rmmsb.v03.n02.023.01



This open access article is licensed under a Creative Commons Attribution International (CC BY 4.0) <http://creativecommons.org/licenses/by/4.0/>.  
Support:

## ABSTRACT

In this work, we analyze the spread of an infectious disease in a not necessarily homogeneous multipopulation that interacts and is distributed in a discrete two-dimensional lattice (network) that acquires only partial immunity to the circulating stain. We use the solution properties of the proposed model to motivate the effects of including space in the dynamics. We show that the dynamics is largely influenced by the topology of the interactions between the different populations. The theoretical results are investigated numerically.

### Keywords:

Partial immunity, Multi-Population SIRC, Spatially distributed, Coupled Map Lattice (CML)

---

## RESUMEN

En este trabajo analizamos la propagación de una enfermedad en una multipoblación no necesariamente homogénea que interactúa y se distribuye en una red discreta bidimensional que adquiere solo inmunidad parcial a la mancha circulante. Usamos las propiedades de solución del modelo propuesto para motivar los efectos de incluir el espacio en la dinámica. Mostramos que la dinámica está influenciada en gran medida por la topología de las interacciones entre las diferentes poblaciones. Los resultados teóricos se investigan numéricamente.

### Palabras Claves:

Inmunidad parcial, SIRC multipoblación, Distribución espacial, Red de mapas vinculados

---

**2020 AMS Mathematics Subject Classification:** Primary: 92B05; Secondary: 92D30, 92C42

## 1 INTRODUCTION

Infectious diseases are caused by infectious agents or pathogens, such as bacteria, viruses, and fungi, which make their host sick. Most of these pathogens can undergo genetic mutations, known as variants or mutating strains, that increase their spread power, resistance, or pathogenicity (ability to cause symptoms), virulence (intensity of host harm), and risk to the human population, see, for example, Hethcote (2000); Casagrandi *et al.* (2006) and references therein.

The emergence of such mutating strains makes it possible for contagion to occur again even if the host has already had contact with the virus, as the immune system does not recognize these variants. In this situation, the host acquires only temporary immunity, also known as cross-immunity, e.g. Casagrandi *et al.* (2006). Infectious diseases with the ability to mutate strains include the Influenza-type and the Sars-Cov-2, e.g., Andraesen (2020); Grifoni *et al.* (2020); Casagrandi *et al.* (2006) and references.

Since the pioneer work of Bernoulli (1760), mathematical models have gained more and more visibility as a tool for testing biological hypotheses in disease dissemination. Particularly, the effects of their strain mutations over time, for example, Diekmann *et al.* (1995); Casagrandi *et al.* (2006).

Once most infectious diseases pass from an infected host to a susceptible one due to some kind of contact, the model prediction will strongly depend on the probability of contact between susceptible and infected individuals. If the population is assumed to be homogeneous, that is, the probability of contact between susceptible and infectious individuals is the same in the total population, then the so-called SIRC model (Susceptible, Infected, Recovered, Cross Immune), proposed in Casagrandi *et al.* (2006), has become a well-accepted model that includes the assumption of cross immunity (a proportion of individuals that acquire only partial immunity to the undergoing disease Casagrandi *et al.* (2006)) over the well-known SIR-type models Hethcote (1989, 2000); Brauer *et al.* (2019).

Most populations are not well mixed due to factors such as geographical and social barriers, social and work activities, and public transportation, to name a few. As a result, the contact probability among individuals in the total population is non-homogeneous. However, the nonhomogeneous nature of population mixing does not mean that this is a random process; see Sattenspiel and Dietz (1995) and the references therein. Nonrandom mixing among spatially distributed subpopulations has many consequences for the outcomes of disease spread, for example Sattenspiel and Dietz (1995); Lazo and De Cezaro (2021); Rossato *et al.* (2021); Marques *et al.* (2022a) and references therein.

A common approach to analyzing the spatial spread of infectious diseases is modeling by discrete temporal population models, or metapopulation models, for example Rossato *et al.* (2021); Brauer *et al.* (2019); Marques (2019), and references therein. Although there are a significant number of recent references in the literature, for example, Brauer *et al.*

(2019) and references therein, continuous-time mathematical models with spatially distributed populations are less common than discrete epidemiological models.

In Sattenspiel and Dietz (1995), the authors investigate the effects of migration dynamics coupling in a continuous-time multi-population SIR model. In Lazo and De Cezaro (2021) and Marques *et al.* (2023) the emerging of a plateau-like shape of the infected population is analyzed due to the mixed interaction in a multi-population SIR model without migration. In Gomes and De Cezaro (2022), a multi-population SIRD-type model was proposed to analyze the effects of COVID-19 on an age-distributed population as a consequence of the reopening of schools. The well-posedness and numerical simulations for a fractional SIRC model with two populations that interact were presented in Maurmann *et al.* (2023). The simulations presented in Maurmann *et al.* (2023) suggest that the existence of immunological memory in both subpopulations induces a favorable epidemiological situation, with fewer infections and fewer cross-immunities. In Marques *et al.* (2022b), the authors analyze a multi-population SIRC type model numerically. Numerical simulation scenarios were analyzed in which the effect of disease reintroduction after a period of time was simulated, simulating the emergence of a new strain. The simulations presented show a tendency to continue to grow in cross-immunity due to the reinfection.

**Main contributions and paper organization:** In this contribution, we explore the effects of inclusion of space in the diseases dynamics of the SIRC-type multipopulation model. The proposed SIRC-type model under investigation assumes the existence of different (not necessarily homogeneous) multipopulation interacting and distributed in a discrete two-dimensional grid (network). We used the smoothness and monotonic behavior of the solution of the SIRC model with multiple populations to show that the spread velocity and intensity of the disease in the network are monotonically dependent on the neighborhood topology (denoted by  $V_{i,j}$ , see below) and the intensity of the interaction (denoted by  $\beta_{i,j}$ , see below). The theoretical results are examined numerically, providing some clues to the mechanisms of disease spread, loss of host immunity, or partial transient immunity in inhomogeneous populations. Understand the dynamics behavior of diseases in spatial distributed and non-homogeneous populations are essential for surveillance by public health authorities, who propose preventive measures and vaccination strategies to mitigate the impact of an emerging disease.

In Section *Model description and its well-posedness*, we present the spatially distributed multipopulation SIRC model and prove its well-posedness. In Section *The effect of introducing space in the disease dynamics*, we used the behavior trajectory and the smoothness properties of the existing solution for the proposed model to motivate the effects of the introduction of space in the dynamics of diseases. In particular, we show that the diffusion velocity and intensity of diseases are monotonically dependent on the neighborhood topology and interaction intensity between the distinct popu-

lations in the lattice. The results are numerically verified in Subsections *Scenario 1* and *Scenario 2*.

## 2 MODEL DESCRIPTION AND ITS WELL-POSEDNESS

We assume the existence of a two-dimensional lattice (nomenclature derived from the theory of Coupled Map Lattice (CML) Marques (2019), where each patch (also known as site pixel or cells)  $(x_i, x_j)$  is represented by integer coordinates (with  $x_i = is, x_j = js$ , where  $s$  is the size of the site), for  $i \in \{1, \dots, k\}, j \in \{1, \dots, n\}$ . In each one of the  $(n \times k)$  patches is the home of a distinct, spatially distributed subpopulation, in which  $N_{i,j}$  represents the individual's density (which corresponds to the total number of individuals in the site). Furthermore, in each of the patches  $(i, j)$ , the density of individuals  $N_{i,j}$  in the subpopulation is proportionally distributed, at any time  $t \geq 0$ , in the susceptible compartments  $S_{i,j}(t)$ , infectious (infected)  $I_{i,j}(t)$ , recovered (removed)  $R_{i,j}(t)$  and cross-immunity  $C_{i,j}(t)$ . In this case, the proportional cross-immunity of the population refers to individuals who have acquired partial immunity but are susceptible to any mutation of the circulating stain within a short period of time. There is no migration of the population from one site to another, in contrast to the approach in Sattenspiel and Dietz (1995). The infection might occur even in such a situation, due to the interaction between subpopulations during work hours or in public transport. But at the end of the day, everyone is back at his home site, where infections are reported. In other words, the assumption of no migration is satisfied by considering that the interaction between distinct subpopulations occurs in an infinitely small time step relative to the time of the disease dynamics  $t$ , such that individuals from different populations interact and return to their reference sites faster than the time  $t \rightarrow t + \Delta t$  of the disease dynamics.

Therefore, the population  $N_{i,j}$  at each site remains constant for any time  $t \geq 0$ . The disease is transmitted from infected individuals to susceptible individuals by the following mechanisms: i) If they belong to the same site, then transmission is proportional to the constant contact rate  $\beta_{i,j} > 0$ , ii) Another source of transmission occurs by contact between susceptible individuals at the site  $(i, j)$  with infected individuals in the neighborhood  $V_{i,j} := \{\text{sites } (\hat{i}, \hat{j}) : (\hat{i}, \hat{j}) \neq (i, j)\}$ . We assume that the transmission between individuals of different populations is proportional to the constant contact rate  $\beta_{\hat{i},\hat{j}} > 0$  if  $(\hat{i}, \hat{j}) \in V_{i,j}$  or  $\beta_{\hat{i},\hat{j}} = 0$  if  $(\hat{i}, \hat{j}) \notin V_{i,j}$ . Therefore, the neighborhood  $V_{i,j}$  determines the topology of contact among different subpopulations in the network, and the parameter  $\beta_{\hat{i},\hat{j}}$  is related to the intensity of interaction with the nearby population.

In the following, we represent the proportion of the infected neighborhood as

$$II := \sum_{\hat{i}, \hat{j} \in V_{i,j}} \beta_{\hat{i},\hat{j}} I_{\hat{i},\hat{j}}(t). \tag{1}$$

Hence,  $S_{i,j}II$  is the probability that susceptible individuals

from the site  $(i, j)$  become infected due to contact with individuals from some of neighboring sites in  $V_{i,j}$ , with rate of contagion  $\beta_{\hat{i},\hat{j}}$ .

We assume that disease dynamics is modeled by a spatially distributed multi-population SIRC-type model, with a normalized and constant total population  $N_{i,j}$ . Using the mass-action law, the dynamics is given by

$$\begin{aligned} \dot{S}_{i,j} &= \mu_{i,j}(N_{i,j} - S_{i,j}) - S_{i,j}(\beta_{i,j}I_{i,j} + II) + \gamma_{i,j}C_{i,j} \\ \dot{I}_{i,j} &= S_{i,j}(\beta_{i,j}I_{i,j} + II) + \sigma_{i,j}\beta_{\hat{i},\hat{j}}C_{i,j}I_{i,j} - (\mu_{i,j} + \alpha_{i,j})I_{i,j} \\ \dot{R}_{i,j} &= (1 - \sigma_{i,j})\beta_{i,j}C_{i,j}I_{i,j} + \alpha_{i,j}I_{i,j} - (\mu_{i,j} + \delta_{i,j})R_{i,j} \\ \dot{C}_{i,j} &= \delta_{i,j}R_{i,j} - \beta_{i,j}C_{i,j}I_{i,j} - (\mu_{i,j} + \gamma_{i,j})C_{i,j}. \end{aligned} \tag{2}$$

In (2), the parameters  $\alpha_{i,j} > 0, \delta_{i,j} > 0, \gamma_{i,j} > 0$  are the inverse of the time that any individual remains in the compartments  $I_{i,j}, R_{i,j}$  and  $C_{i,j}$ , respectively, for  $i = 1, \dots, n$  and  $j = 1, \dots, k$ . The parameter  $\sigma_{i,j}$  is the probability of reinfection, while the parameter  $\mu_{i,j} > 0$  represents the mortality/birth rate, which we assume to be equal for all subpopulations.

Furthermore, the model given in (2) is considered with the following initial conditions  $X_{i,j}(0) := (S_{i,j}(0), I_{i,j}(0), R_{i,j}(0), C_{i,j}(0))^T \in \mathcal{R}_+^4 := \{X_{i,j}(t) := (S_{i,j}(t), I_{i,j}(t), R_{i,j}(t), C_{i,j}(t))^T \in \mathcal{R}^4 : S_{i,j}(t) \geq 0, I_{i,j}(t) \geq 0, R_{i,j}(t) \geq 0, C_{i,j}(t) \geq 0, t \geq 0\}$ , for  $i \in \{1, \dots, k\}, j \in \{1, \dots, n\}$ .

**Note 1** *The model given in (2) is a generalization of the SIRC model proposed by Casagrandi et al. (2006) for multi-populations that spatially interact without migration dynamics; see Sattenspiel and Dietz (1995). In fact, if all subpopulations are isolated, which is equivalent to setting  $II = 0$  in (2) (or equivalently  $\beta_{\hat{i},\hat{j}} = 0$  for all sites  $(\hat{i}, \hat{j}) \in V_{i,j}$ ), we have the SIRC model originally proposed in Casagrandi et al. (2006), for each of the subpopulations. As a result, the term  $S_{i,j}II$  in the model given in (2) is related to the probability that susceptible individuals from the site  $(i, j)$  become infected due to contact with individuals from neighboring sites in  $V_{i,j}$ , but without migration.*

*It is worth mentioning that the specification of  $V_{i,j}$  and  $\beta_{\hat{i},\hat{j}}$  determines the topology of the multipopulation interaction in the network. In particular, restriction on  $V_{i,j}$  and  $\beta_{\hat{i},\hat{j}}$  (for example,  $\beta_{\hat{i},\hat{j}} = 0$  represents the isolation of subpopulation) and can be seen as a control strategy. In this case, if a disease starts in a subpopulation, it will become confined in such a population, insofar as there is no interaction between different subpopulations ( $\beta_{\hat{i},\hat{j}} = 0$ ), see Marques et al. (2022a) and the references therein. If the network size is too small or  $V_{i,j}$  contains as many neighborhood sites, then the model dynamics given in (2) is expected to behave as a single population model with a variable transmission rate  $\beta_{i,j}$ . See also the discussion in the next section. The topology of the multipopulation interaction is the main subject of the numerically simulated scenarios in Section numerically simulated scenarios.*

*The assumption of non-migratory dynamics and the birth / mortality rates to be constant implies that the number of in-*

dividuals in each subpopulation  $N_{i,j}$  remains constant. The nonmigration assumption allows us to analyze the effects of the neighborhood interaction topology analytically, as shown in Section Effects of introducing space in the disease dynamics. However, it is one of the weaknesses of the proposed model. We aim to analyze the model given in (2) with some migration patterns, for example, the one proposed in Sattenspiel and Dietz (1995) in future contributions.

In the following, we present the well-posedness of the model given in (2), which supports the forthcoming analysis and the numerically simulated scenarios and their interpretations presented in Section Numerical simulated scenarios.

**Theorem 1** *Let the parameters of the model given in (2) be constant and the initial conditions given by  $X_{i,j}(0)$ . Then, there exists a unique, continuously differentiable and non-negative solution  $X(t)$  (a vector with  $n \cdot k$  coordinates corresponding to  $(S_{i,j}(t), I_{i,j}(t), R_{i,j}(t), C_{i,j}(t))$ , for all,  $i = 1, \dots, n, j = 1 \dots, k$ , with non-negative coordinates) for any  $t \in [0, +\infty[$ , that continuously depends on the model parameters and initial conditions.*

*Sketch of the Proof:* Since there is no migration, then summing over all the equations in the model given in (2), it follows that the total population at each site remains constant for all  $t$ . As a result,  $S_{i,j}, I_{i,j}, R_{i,j}$  and  $C_{i,j}$  are uniformly bounded. Therefore, the Jacobian matrix corresponding to the right-hand side of model defined in (2) is uniformly bounded. Then, from the Mean Value Theorem Hale (1980) we see that the right-hand side of (2) is right-hand continuous with respect to  $t$  and Lipschitz continuous with respect to  $S_{i,j}, I_{i,j}, R_{i,j}$  and  $C_{i,j}$ , for  $i = 1, \dots, n, j = 1, \dots, k$ . The continuity of  $S_{i,j}, I_{i,j}, R_{i,j}$  and  $C_{i,j}$ , for  $i = 1, \dots, n, j = 1, \dots, k$ , also follows straightforward arguments. It follows from classical results on dynamical systems, e.g., Hethcote (2000), the existence of a unique smooth and positive solution  $X(t)$  as stated in the Theorem, in the interval  $[0, T]$ , for some  $T > 0$ . Since the solution is uniformly bounded by  $N_{i,j}$ , it follows that the right-hand side of the system proposed in (2) can be bounded by an affine function depending only on the solution of the model  $X(t)$  and the model parameters. Therefore, using the classical results of the dynamical system Hale (1980), the solution can be continuously extended to the positive real line.  $\square$

### 3 EFFECTS OF INTRODUCING SPACE IN THE DISEASE DYNAMICS

In this section, we address some interesting conclusions about some of the effects of space inclusion in disease diffusion dynamics based on the behavior and properties of the solution of the model given in (2).

First, it should be noted that Theorem 1 implies that  $II$  (defined in (1)) is a monotonically increasing function of the neighborhood topology  $V_{i,j}$  and its intensity  $\beta_{i,\hat{j}}$ , at any given time  $t \geq 0$ , as a result of  $I_{i,j}(t) \geq 0$ .

Hence, from the first equation in the model given in (2), we can see that  $S_{i,j}(t)$  remains a decreasing function of  $t$  whenever

$$C_{i,j} \leq \frac{(S_{i,j}(\beta_{i,j}I_{i,j} + II) - \mu_{i,j}(N_{i,j} - S_{i,j}))}{\gamma_{i,j}}. \tag{3}$$

In the early stages of the diseases,  $C_{i,j} = C_{i,j}(0) = 0$  or  $I_{i,j} = 0$  (in the remaining non-infected sites).

The basic reproduction number<sup>1</sup>

In any case, if the neighborhood  $V_{i,j}$  is not empty and has some proportion of infected individuals such that  $\mathcal{R}_0^{(i,j)} > 1$ , then it follows from the second equation of the model given by (2) that  $I_{i,j}$  will increase. Since  $N_{i,j}$  is constant, it follows that  $I_{i,j}(t) < \infty$ , for all  $t \geq 0$ .

As a result of the properties mentioned above and the smoothness of  $I_{i,j}(t)$  (see Theorem 1), we conclude that there will be a solution trajectory for  $I_{i,j}(t)$  (depending on the neighborhood topology of  $II$ ) that has a concave hump, as shown in Figure 4-a). Therefore,  $I_{i,j}(t)$  reaches its maximum at a point  $t_p^{i,j} \in ]0, +\infty[$ , known as the turning point, within  $I_{i,j}(t_p^{i,j}) \neq 0$ . From the maximality of  $I_{i,j}$  at  $t_p^{i,j}$  we have  $\dot{I}(t_p^{i,j}) = 0$ . Hence, from the second equation in the model given by (2) that

$$S_{i,j}(t_p^{i,j}) = \frac{(\mu_{i,j} + \alpha_{i,j}) - \sigma_{i,j}\beta_{i,j}C_{i,j}(t_p^{i,j})}{\beta_{i,j}} \left( \frac{1}{1 + \frac{II(t_p^{i,j})}{\beta_{i,j}I_{i,j}(t_p^{i,j})}} \right). \tag{5}$$

The analysis of equation (5) reveals some possibilities whose consequences is worth exploring is as follows:

- i) In the first analysis, (3) implies that  $C_{i,j}$  increases with  $II$ . On the other hand, since the number of susceptibles is always non-negative (see Theorem 1), then (5) implies the following threshold for the cross-immunity, given by

$$C_{i,j}(t_p^{i,j}) \leq \frac{(\mu_{i,j} + \alpha_{i,j})}{\sigma_{i,j}\beta_{i,j}}. \tag{6}$$

Such bound is independent of the neighborhood topology. This phenomena is observed numerically in Figures 2 and 4-b).

<sup>1</sup>Quantity that expresses the expected number of cases directly generated by one case in a population and within the selected population at the initial phase of the infection Diekmann (1990); van den Driessche and Watmough (2002). of the population  $(i, j)$ , calculated using the next generation matrix Diekmann (1990); van den Driessche and Watmough (2002), is given by

$$\mathcal{R}_0^{(i,j)} = (\mu_{i,j} + \alpha_{i,j})^{-1} \left( \beta_{i,j} + \sum_{\hat{i}, \hat{j} \in V_{i,j}} \beta_{\hat{i}, \hat{j}} \right). \tag{4}$$

Therefore, we can have  $\mathcal{R}_0^{(i,j)} > 1$ , even when the basic reproductive number of totally isolated subpopulations  $\tilde{\mathcal{R}}_0^{(i,j)} := \frac{\beta_{i,j}}{\alpha_{i,j} + \mu_{i,j}} < 1$  (which corresponds to the case where  $\beta_{\hat{i}, \hat{j}} = 0$ ). As a consequence, the asymptotical stability of the disease-free equilibrium point at a site  $(i, j)$  also depends on the neighborhood topology given in (1), (see the analysis derived in Marques et al. (2023) for the spatially distributed SIR model).



ii) In an isolated population, that is, in a site  $(i, j)$  where  $V_{i,j}$  is empty (or  $\beta_{i,\hat{j}} = 0$ ), then the number of susceptibles at  $t_p^{i,j}$  is

$$S_{i,j}(t_p^{i,j}) = \frac{(\mu_{i,j} + \alpha_{i,j}) - \sigma_{i,j}\beta_{i,\hat{j}}C_{i,j}(t_p^{i,j})}{\beta_{i,j}}. \quad (7)$$

iii) Increasing the network topology  $V_{i,j}$  or the intensity interaction  $\beta_{i,\hat{j}}$ , causes  $S_i(t_p^i)$  to decrease (since the denominator in (5) increases), and therefore  $I(t_p^i)$  increases. Figures 1, 10 and 12 depicted this situation.

iv) As a consequence of items ii) and iii),  $S_i(t_p^{i,j})$  remains at its highest possible value in the scenario where there is minimal interaction between populations and cross-immunity.

The effects of introducing space into the model dynamics proposed in (2) and its relation to above-mentioned situations i), ii), iii) and iv) will be addressed numerically in the following subsection.

#### 4 NUMERICAL SIMULATED SCENARIOS

In this subsection, we investigate numerically the effect that the interaction between distinct subpopulations following the dynamics given in (2) has on the disease dynamics that reflect the situations i), ii), iii) and iv) described above. In all the presented simulations, the solution  $X(t)$  of the model given in (2) is numerically obtained using the Euler method with a step-size of  $h = 10^{-4}$  that guarantee the numerical accuracy of the approximation and avoids the stiffness phenomena, see da Silva *et al.* (2023.No Prelo). The network has  $14 \times 14$  sites, which means that  $n = k = 14$ . Furthermore, the parameters  $\alpha_{i,j} = 52.14$ ,  $\delta_{i,j} = 0.75$ ,  $\mu_{i,j} = 0.00001$ ,  $\gamma_{i,j} = 0.35$  and  $\sigma_{i,j} = 0.12$ , for  $i, j \in \{1, \dots, 14\}$ , based on the parameters given in Casagrandi *et al.* (2006), are kept fixed in all simulations. Therefore, as previously announced in Remark 1, we shall see below the effects of the neighborhood of interaction topology  $V_{i,j}$  and its intensity given by the parameter  $\beta_{i,\hat{j}}$  on the disease behavior for the infected and cross-immunity portions of each of the populations.

##### SCENARIO 1: EFFECTS ON DISEASE DYNAMICS DUE TO VARIATION OF THE DISTINCT POPULATION INTENSITY INTERACTION $\beta_{i,\hat{j}}$ , WHILE THE NEIGHBORHOOD OF INTERACTION TOPOLOGY $V_{i,j}$ IS KEPT FIXED

In all simulations presented in this first scenario, we assume that each population located in the patch  $(i, j)$  of the lattice interacts only with the four neighbors in a rectangular vicinity  $V_{i,j}$  that has a common face interception, also called the Neumann-type neighborhood, e.g. Marques (2019). In Figures 1 and 2, we see the effects on the dynamics of the total infected and cross-immunity population for different choices of interaction intensity  $\beta_{i,\hat{j}} \neq 0$  for  $(i, \hat{j}) \in V_{i,j}$  and zero elsewhere. More specifically, in all simulated scenarios, we have:

- 1) The density  $N_{i,j}$  is constant, corresponding to a total population of 100 individuals in all the  $14 \times 14$  patches;
- 2) Infection starts at two distinct sites simultaneously at  $t = 0$ . They correspond to the sites of the positions (10,5) and (5,11) in the lattice. The total number of infected individuals in such patches is  $I_{10,5}(0) = I_{5,11}(0) = 20$ .
- 3) The initial conditions  $X_{i,j}(0)$  are such that  $S_{i,j}(0) = 100$  and  $I_{i,j} = 0$  if  $(i, j) \neq (10,5)$  or  $(i, j) \neq (5,11)$  and  $S_{10,5} = S_{5,11} = 80$  (see item 2) and  $R_{i,j}(0) = C_{i,j}(0) = 0$  in all patches.
- 4) The distinct population interaction intensity is such that  $\beta_{i,\hat{j}} = \beta_{i,j}/\kappa$  in  $V_{i,j}$  and  $\beta_{i,\hat{j}} = 0$ , otherwise, the values of  $\kappa$  are chosen for simulated sub-populations with a large or a small interaction in the vicinity  $V_{i,j}$  as follows:

Case 1,  $\kappa = 15000$ ; It corresponds to  $\beta_{i,\hat{j}} = 0.00783$  and is the lower intensity interaction in the simulated scenarios.

Case 2,  $\kappa = 1500$ ; It corresponds to  $\beta_{i,\hat{j}} = 0.0783$  and is the middle-lower intensity interaction in the simulated scenarios.

Case 3,  $\kappa = 150$ ; It corresponds to  $\beta_{i,\hat{j}} = 0.783$  and is the middle-large intensity interaction in the simulated scenarios.

Case 4,  $\kappa = 15$ . It corresponds to  $\beta_{i,\hat{j}} = 7.83$  and is the large intensity interaction in the simulated scenarios.

In Figures 1-4, we presented the simulated scenarios using the settings of this subsection. It is possible to see in Figure 1 that in Case 1 and 2 for the choices of  $\beta_{i,\hat{j}}$  the total infected proportion of the population presents an oscillatory behavior due to the time it takes for the diseases to spread between different sites (compare with equation (5)). This behavior is not observed for the interaction of medium-large and high intensity  $\beta_{i,\hat{j}}$ , because in such cases the spread velocity of the diseases between different populations is large, see red and pink curves in Figure 1 (since  $\kappa$  is large in (5)). The intensity of interaction between different populations  $\beta_{i,\hat{j}}$  is also monotonically related to the proportion of the infected population at the time of selection of infection (see Figure 1 and compare with Equation (5)). Monotonic behaviors are reflected in the proportion of cross-immunity of the population in terms of the choices for  $\beta_{i,\hat{j}}$ , as presented in Figure 2. The spatial distribution of the cross immunology for Case 1 at time  $t = 0.4$  and Case 4 at time  $t = 0.25$  is presented in Figure 3 on the right side. As can be observed in Figure 3, the cross-immunity front wave does not cover the lattice in Case 1, but has fulfilled all the patches for Case 4, even considering an earlier time for the last case. Such a behavior implies that cross-immunity achieves stability early for a large distinct population interaction  $\beta_{i,\hat{j}}$ , as presented in Figure 2. A similar distribution can be observed in the

infected population Figure 3 on the left.

In Figure 4, we show the evolution of the dynamics for infected and cross-immunity populations in different lattice patches for the intensity of interaction, representing Cases 1 and 4, respectively. The main difference in infected populations is the time at which the peaks occur (see also (5)). At the patch (5, 11) where the disease started, we observe the first and more intense peak (see the Figure 4(a)). Another interesting fact is the time interval in which the dynamics between sites occurs when comparing cases 1 and 4. When there is more interaction (Case 4), the time interval between one curve and another is much shorter than in Case 1, in other words, the diffusion of the disease in the space is faster (see the  $\mathcal{R}_0^{i,j}$  in (4)).

## SCENARIO 2: EFFECTS ON THE DISEASES DYNAMICS DUE TO VARIATION OF NEIGHBORHOOD TOPOLOGY $V_{i,j}$

In this subsection, we present numerical simulation scenarios for distinct choices of the neighborhood topology  $V_{i,j}$  and will discuss its effect on the dynamics of the disease. In particular, it shows another point of view of the effects of the space interaction on the dissemination of diseases. The results presented in Figures 10- 13 show the distinct dynamics of disease dissemination in the following neighborhoods:

- *Neumann neighborhood*: In such a neighborhood, each population (patch) interacts only with the four neighbors in a rectangular vicinity  $V_{i,j}$  that has a common face of interception (see Figure 5);
- *V neighborhood*: In such a neighborhood, each population (patch) interacts only with the eight neighbors in a plus-shaped (not rectangular) vicinity  $V_{i,j}$  (see Figure 6);
- *V\* neighborhood*: In such a neighborhood, each population (patch) interacts only with the eight neighbors in a plus-shaped (not-rectangular) vicinity  $V_{i,j}$  but the intensity of the distinct population interaction  $\beta_{\hat{i},\hat{j}}$  is 1/2 of the neighbor site that has a common face interception (see Figure 7);
- *Moore neighborhood*: In such a scenario, each population (patch) interacts with the eight neighbors in a rectangular vicinity  $V_{i,j}$  (see Figure 8);
- *Moore\* neighborhood*: This is a variation of the Moore neighborhood, where we considered that each population (patch) interacts with the eight neighbors in a rectangular vicinity  $V_{i,j}$  but, in the absence of a common face interception in the vicinity, the intensity of the distinct population interaction  $\beta_{\hat{i},\hat{j}}$  is 1/2 of the neighbor site that has a common face interception (see Figure 9);

In all simulations presented in this subsection, we used the intensity of interaction between the different subpopulations in the vicinity to be chosen as  $\beta_{\hat{i},\hat{j}} = \beta_{i,j}$  if  $(\hat{i}, \hat{j}) \in V_{i,j}$  and

$\beta_{\hat{i},\hat{j}} = 0$  elsewhere. The remaining parameters of the model given in 2 are the same as those described at the beginning of this section. Therefore, the effect of space throughout the neighborhood topology  $V_{i,j}$  is what makes the analysis different from the SIRC model with homogeneous population analyzed elsewhere in Casagrandi *et al.* (2006). See also the comments on Remark 1.

In Figure 10, we show the dynamics of the infected proportion of the total population for different configurations of  $V_{i,j}$  as explained above. We can observe that for  $V_{i,j}$  with the same number of neighbors, the curves are very close (see the blue and green curves in Figure 10 for example and compare them with equation 5). The proportion of cross-immunity in the population has a more evident peak for smaller neighborhoods (see the blue curve in Figure 11).

We will present two situations for distinct initial conditions, indeed: a) the disease started in two patches, namely the patches (10,5) and (5,11), respectively. For such a scenario, the initial conditions are the same as those described in Subsection *Scenario 1*. b) The disease started in only one patch, namely (5, 11). In such a case, the initial conditions are such that  $I_{10,5} = 0$  and then  $S_{10,5} = 100$ . The remaining initial conditions remain the same as before.

In Figure 12, we show the dynamics of the total infected population in the network due to the distinct choices of the neighborhood and the initial conditions, in three distinct sections of the simulated time intervals. The early dynamics of the infection is presented in Figure 12,-a). It is worth noting that infection pick is monotonically decreasing with the number of neighborhood sites in the vicinity  $V_{i,j}$  and the intensity interaction  $\beta_{\hat{i},\hat{j}}$ . Moreover, it suffers a small shift in time and a considerable decrease in its maximum due to the initial conditions, with the infection beginning at only one site. Figure 12 b) and c) show an oscillating and time shift with the prevalence of the diseases in the long run of the model (2) dynamics, that are independent of the simulated initial conditions. In particular, this result shows that (5) remains true.

In Figure 13, we present the dynamics of the proportion of cross-immunity of the total population, for the simulated scenarios described in this subsection. The simulations presented show that the dynamics of the cross-immunity is independent of the vicinity  $V_{i,j}$  and the initial conditions in the short duration of the diseases (up to  $t = 0.5$ ). Then, it presents a monotonically decreasing behavior with the number of neighborhoods and the intensity interaction  $\beta_{\hat{i},\hat{j}}$  in the neighborhood topology  $V_{i,j}$ . Then it presented and shifted the oscillatory behavior independent of the vicinity topology or initial conditions. Therefore, (6) is numerically verified.

In Figure 14 we present the spatial distribution of the infected population at the beginning of the infection  $t = 0.002$  for different types of neighborhoods. Note that the sites

(subpopulations) already affected by the infection differ significantly in each case. For the type V neighborhood, we observed that the sites with the presence of infected people already exceeded half of the network. This fact is also observable in the Figure 10(a), in which the largest fractions of the affected population correspond to the V and  $V^*$  neighborhoods.

The simulation regarding distinct topologies for vicinity choices shows a monotonically increasing and a shifted pick of infection. Also, there is a monotonically decreasing pick of cross-immunity in the total population with respect to the number of neighbors in the vicinity. This monotonic behavior is also observed due to the number of infected sites in the initial conditions for the total infected populations, but is not observed in the cross-immunity dynamics (see (6) and (5)). The number of neighbors in the vicinity implies a shifting oscillatory behavior and the permanence of the disease infection and cross-immunity in the total population.

## 5 CONCLUSION AND FUTURE DIRECTIONS

In this contribution, we discuss the effects of space inclusion on the behavior dynamics of a disease in which distinct and not necessarily homogeneous interacting multi-populations, distributed in a discrete two-dimensional network, acquire only partial immunity to circulating stain, modeled by a compartmental multi-population SIRC-type model without migration. The properties of the model solution were used to show that the spread velocity and intensity of the disease to reach its peak of infection in the network are monotonically dependent on the topology of the neighborhood  $V_{i,j}$  and the intensity of the interaction  $\beta_{i,j}$ , while the cross-immunity is uniformly bounded independently of such quantities. These theoretical results are examined numerically in some particular cases for neighborhood topology  $V_{i,j}$  and interaction intensity  $\beta_{i,j}$  (see Subsection *Scenario 1-Scenario 2*). As far as the authors are aware, such results were not investigated elsewhere. The results obtained provide some clues about the mechanisms of disease spread and loss of host immunity or transient partial immunity in inhomogeneous populations.

Future developments of this approach include the analysis of equilibrium points and stability.



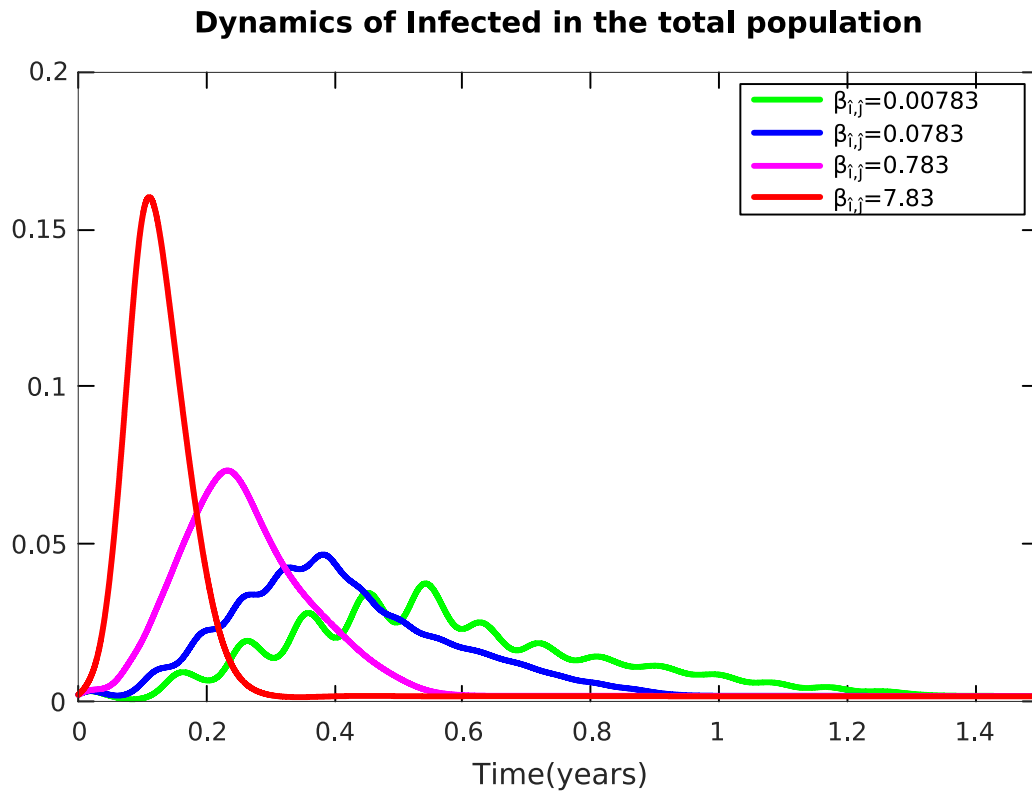


**Figure 1:** The dynamic behavior of the proportion of the total infected population for distinct choices of the intensity of the population interaction in a Neumann type neighborhood.

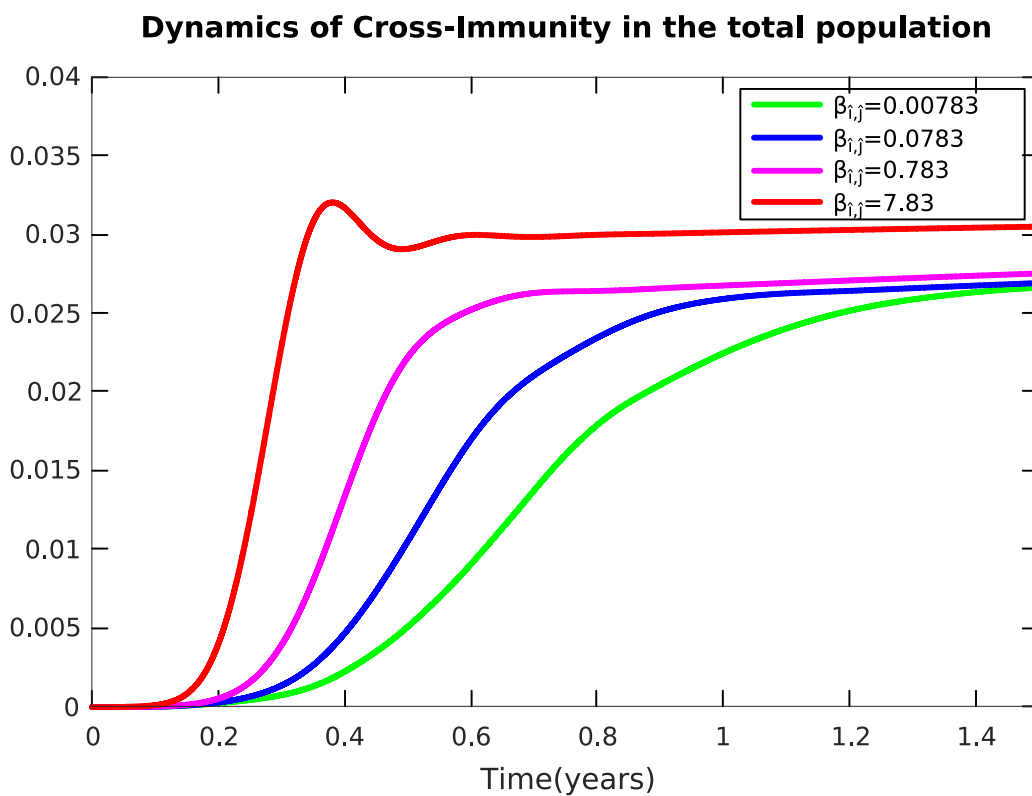
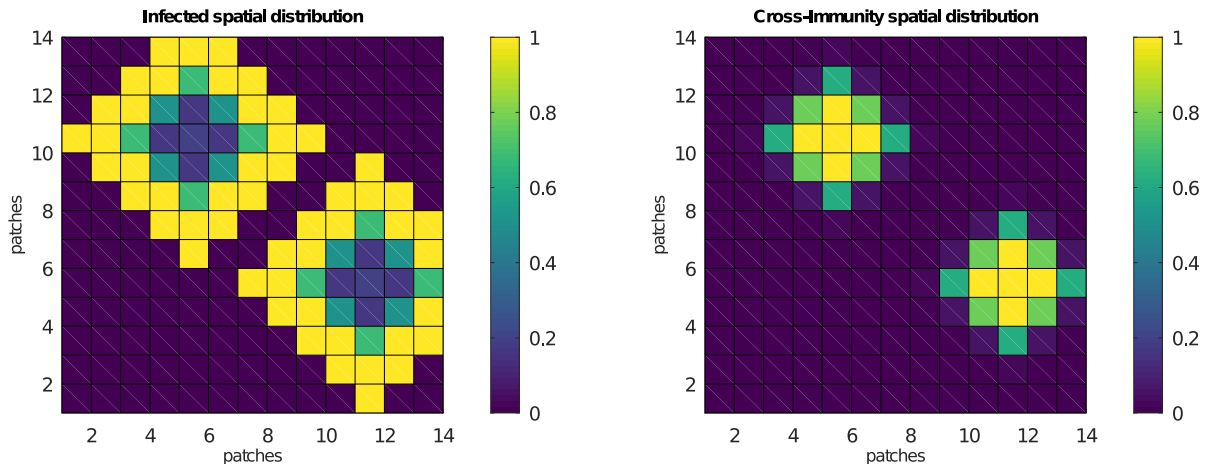
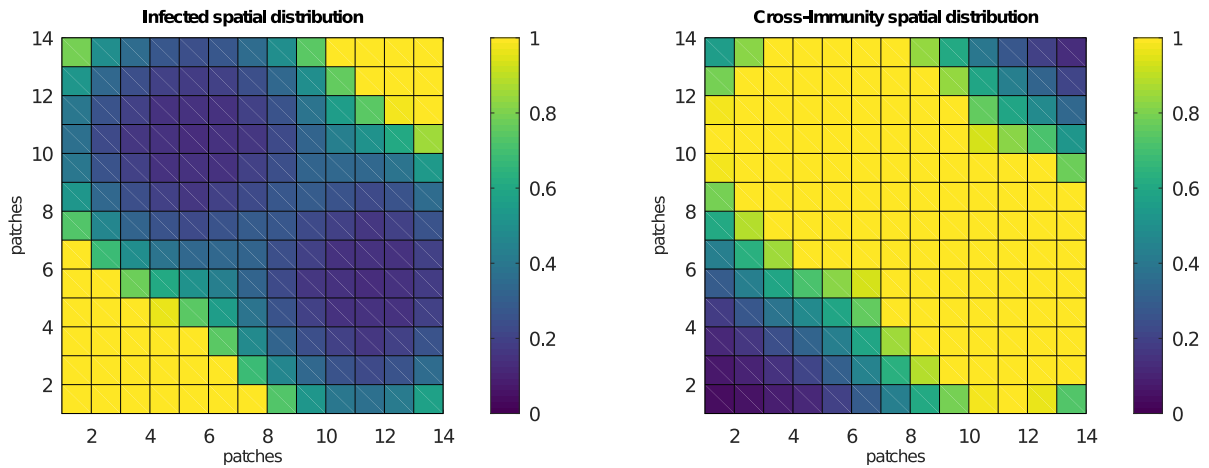


**Figure 2:** The dynamic behavior of the proportion of the total cross-immune population, for distinct choices of the intensity of the population interaction in a Neumann type neighborhood.



(a) Spatial distribution of the infected and cross-immune population in the lattice at time  $t = 0.4$ , in the scenario of lower sub-population interaction, in a Neumann type neighborhood - Case 1.



(b) Spatial distribution of the infected and cross-immune population in the lattice at time  $t = 0.25$  in the scenario of large sub-population interaction in a Neumann type neighborhood - Case 4.

Figure 3

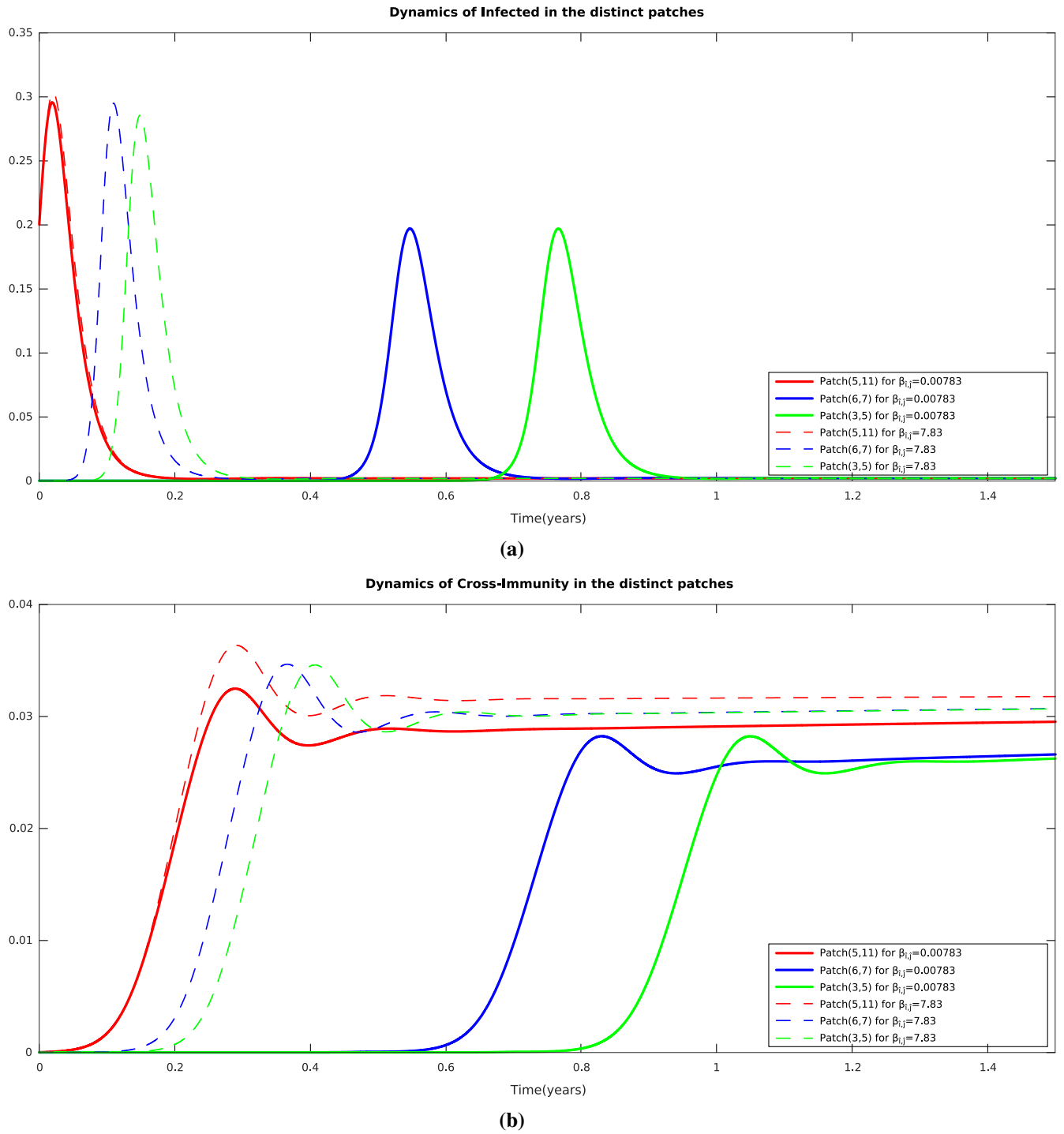


**Figure 4:** (a) The dynamic behavior of the proportion of the infected population in distinct patches for the parameter setting in the scenario 1, for  $\kappa = 1.500$  and  $\kappa = 15$ , respectively. (b) The dynamic behavior of the proportion of the population of the cross-immunity in distinct patches for the parameter setting in scenario 1, for  $\kappa = 1.500$  and  $\kappa = 15$ , respectively.

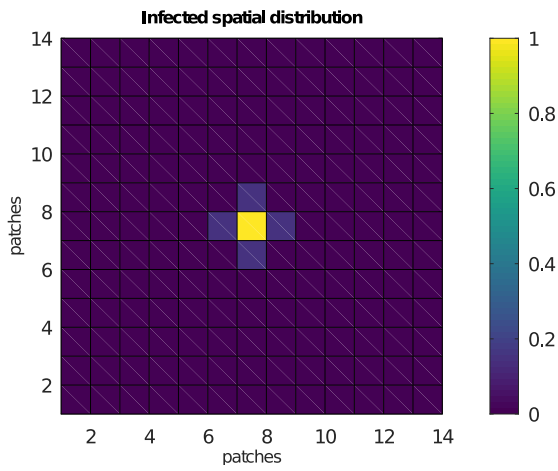


**Figure 5:** An example of spatial distribution in the case of a Neumann neighborhood.

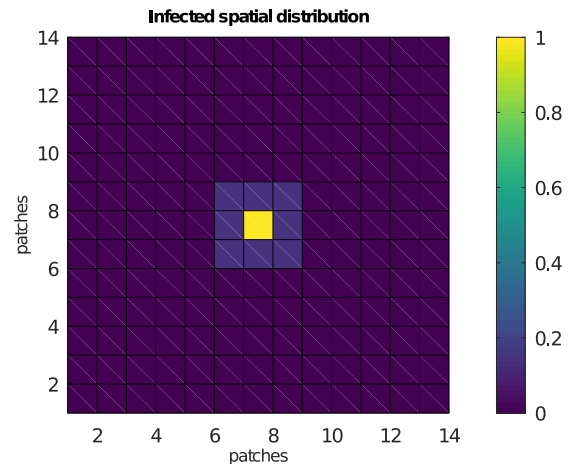


**Figure 8:** An example of spatial distribution in the case of a Moore neighborhood.

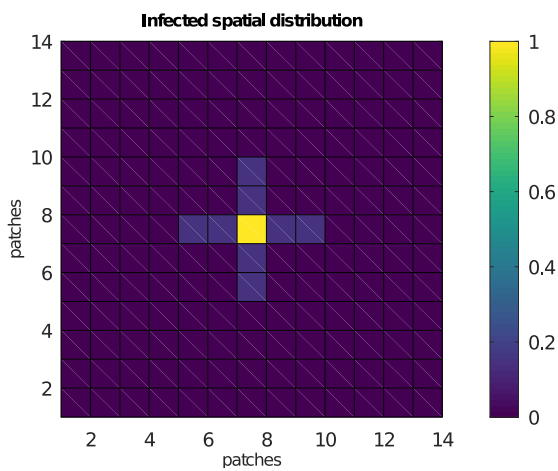


**Figure 6:** An example of spatial distribution in the case of a V neighborhood.

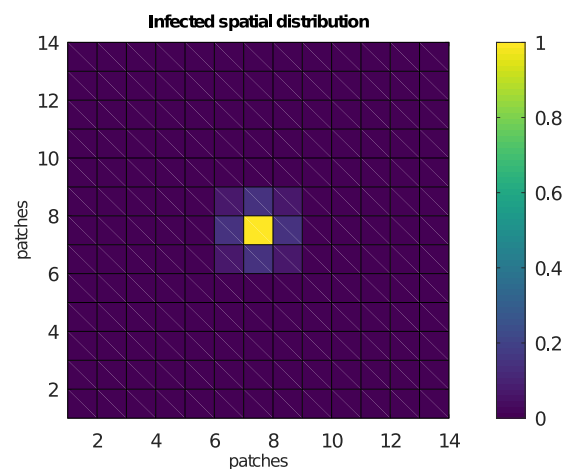


**Figure 9:** An example of spatial distribution in the case of a Moore\* neighborhood.

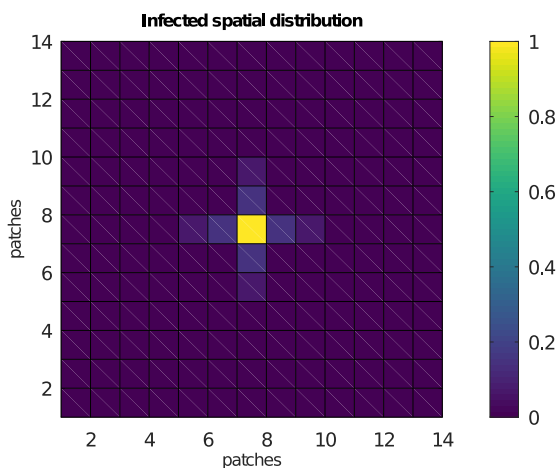


**Figure 7:** An example of spatial distribution in the case of a V\* neighborhood.

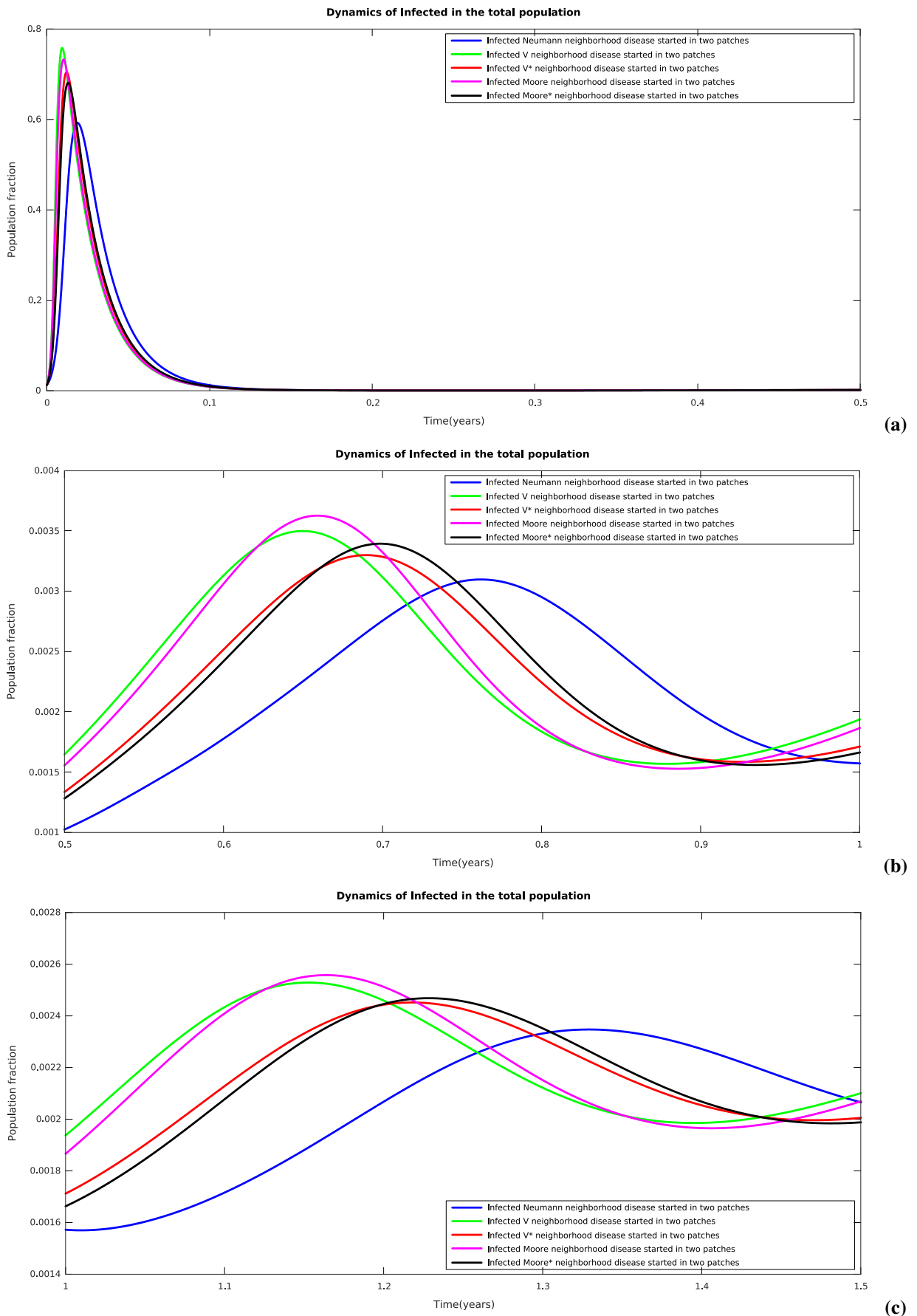


**Figure 10:** The dynamic behavior of the proportion of the total infected population in different time intervals for distinct neighborhoods for the parameter settings and neighborhood of the scenario 2.



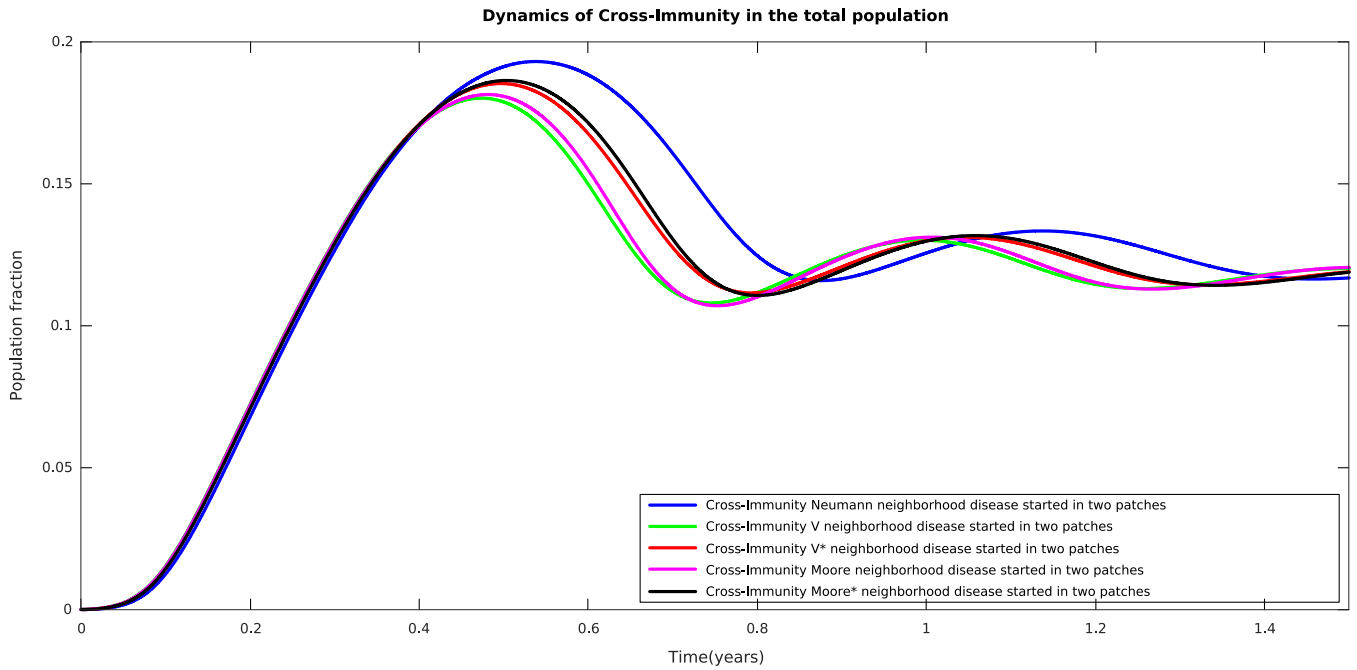


**Figure 11:** The dynamic behavior of the proportion of the total Cross-immunity population for distinct neighborhoods for the parameter settings and neighborhood of the scenario 2.

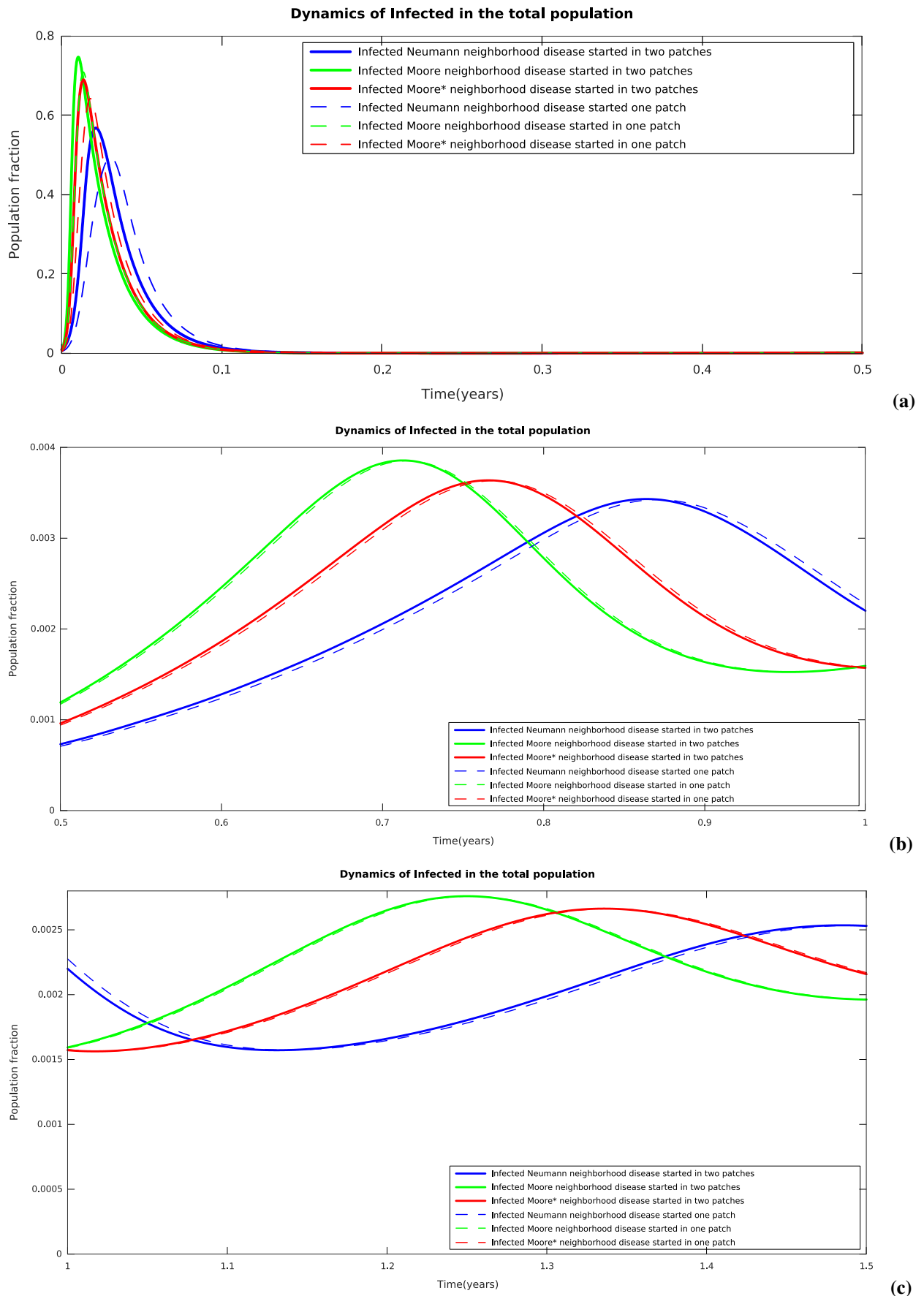


**Figure 12:** The dynamic behavior of the proportion of the total infected population in different time intervals for distinct neighborhoods according to choices a) and b) for the initial conditions and for the parameter settings and neighborhood of the scenario 2.

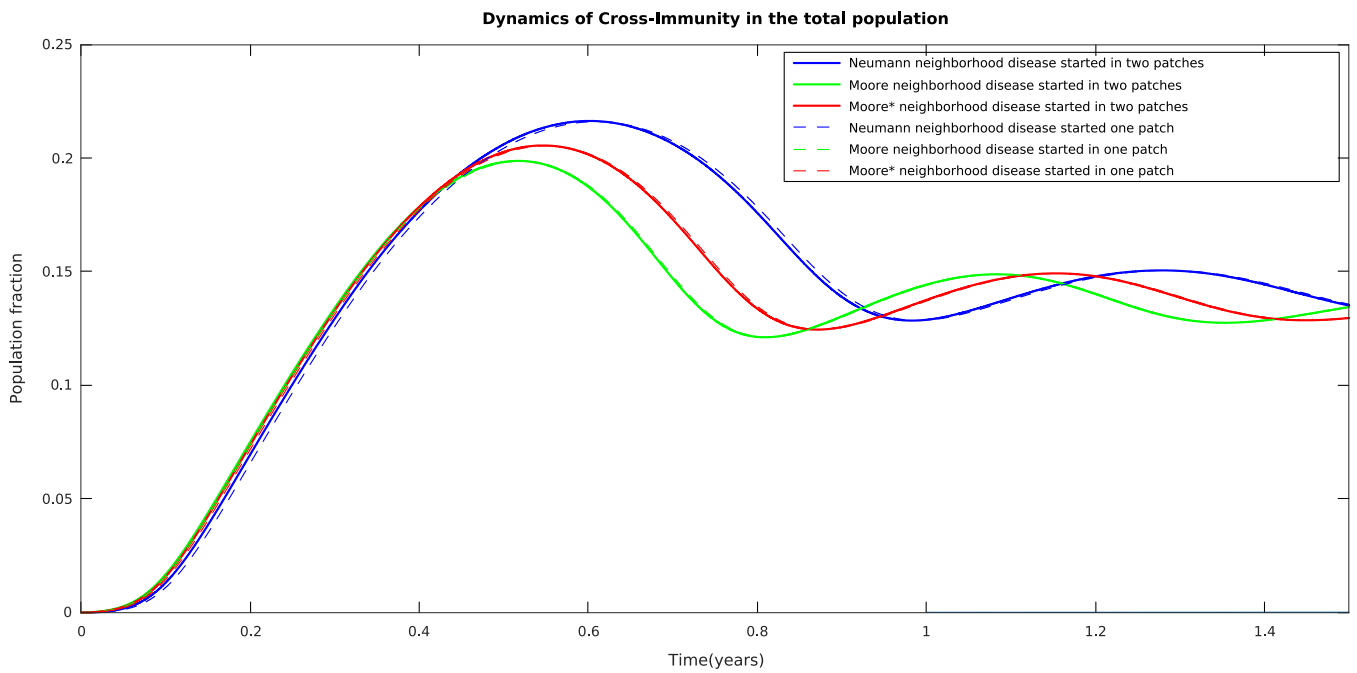


**Figure 13:** The dynamic behavior of the proportion of the total cross-immune population for distinct neighborhoods according to choices a) and b) for the initial conditions and for the parameter settings of scenario 2.

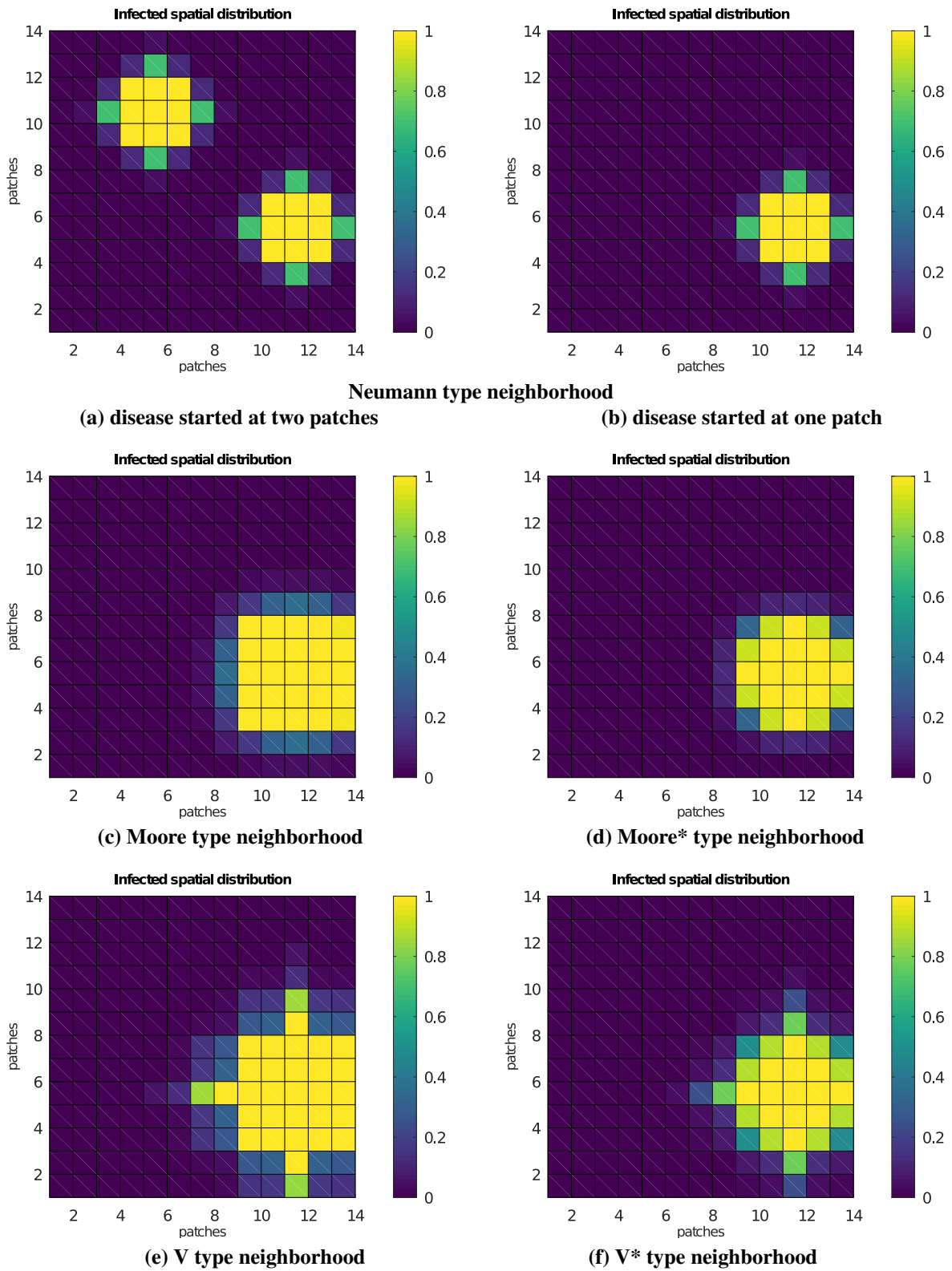


Figure 14: Comparison between different neighborhoods in  $t = 0.002$ .

## REFERENCES

- Andreasen, V.; Gog, J. (2020) 'Pease (1981): The evolutionary epidemiology of influenza a.' *Theoretical Population Biology*, 133, pp. 29–32.
- Bernoulli, D. (1760) 'Essai d'une nouvelle analyse de la mortalité causée par la petite vérole, et des avantages de l'inoculation pour la prévenir'. *Histoire de l'Acad., Roy. Sci.(Paris) avec Mem.*, pp. 1–45.
- Brauer, F., Castillo-Chavez, C. and Z., F. (2019) *Mathematical Models in Epidemiology*. Springer.
- Casagrandi, R. et al. (2006) 'The SIRC model and Influenza A'. *Mathematical Biosciences*, 200(2), pp. 152–169.
- Diekmann, O., H.J.M.J. (1990) 'On the definition and the computation of the basic reproduction ratio  $r_0$  in models for infectious diseases in heterogeneous populations'. *J. Math. Biol.*, 1(28), pp. 365–382.
- Diekmann, O., Metz, J. and Heesterbeek, J.A.P. (1995) 'The legacy of kermack and mckendrick'. *Epidemic Models: Their Structure and Relation to Data Mollison, D. E. (ed.)*, Cambridge University Press, Cambridge., (1).
- Gomes, A.C.F.N. and De Cezaro, A. (2022) 'A model of social distancing for interacting age-distributed multi-populations: An analysis of students' in-person return to schools'. *Trends in Computational and Applied Mathematics*, 23(4), pp. 655–671.
- Grifoni, A., Weiskopf, D., Ramirez, S.I., Mateus, J., Dan, J.M., Moderbacher, C.R., Rawlings, S.A., Sutherland, A., Premkumar, L., Jodi, R.S., Marrama, D., de Silva, A.M., Frazier, A., Carlin, A.F., Greenbaum, J.A., Peters, B., Krammer, F., Smith, D.M., Crotty, S. and Sette, A. (2020) 'Targets of t cell responses to sars-cov-2 coronavirus in humans with covid-19 disease and unexposed individuals'. *Cell*, 181(7), pp. 1489–1501.e15. doi:<https://doi.org/10.1016/j.cell.2020.05.015>. Available at: <https://www.sciencedirect.com/science/article/pii/S0092867420306103>.
- Hale, J.K. (1980) *Ordinary Differential Equations (2nd ed.)*, vol. 1. Malabar: Robert E. Krieger Publishing Company.
- Hethcote, H.W. (1989) 'Three basic epidemiological models'. In *Applied mathematical ecology*. Springer, pp. 119–144.
- Hethcote, H.W. (2000) 'The mathematics of infectious diseases'. *SIAM Review*, 42(4), pp. 599–653.
- Lazo, M.J. and De Cezaro, A. (2021) 'Why can we observe a plateau even in an out of control epidemic outbreak? a seir model with the interaction of n distinct populations for covid-19 in brazil.' *Trends in Computational and Applied Mathematics*, 22(1), pp. 109–123.
- Marques, J.C. (2019) *Modelos para dispersão de javalis { Sus scrofa }*. Ph.D. thesis, Universidade Federal do Rio Grande do Sul.
- Marques, J.C., De Cezaro, A. and Lazo, M.J. (2022a) 'A sir model with spatially distributed multiple populations interactions for disease dissemination'. *Trends in Computational and Applied Mathematics*, 23(1), pp. 143–154.
- Marques, J.C., De Cezaro, A. and Lazo, M.J. (2023) 'On an emerging plateau in a multi-population sir model'. *preprint*, (1), pp. 1–21.
- Marques, J.C., Gomes, A.C.F.N. and De Cezaro, A. (2022b) 'A numerical study of the effect of population interaction on disease dissemination and cross immunity'. In: *McSul*, 9, formato virtual.
- Maurmann, A.C., Travessini De Cezaro, F. and De Cezaro, A. (2023) 'A fractional sirc model for the spread of diseases in two interacting populations'. *LATIN-AMERICAN JOURNAL OF COMPUTING*, to appear, pp. 1–8.
- Rossato, M.C., RODRIGUES, L.A.D. and Mistro, D.C. (2021) 'Padrões espaciais de agregação populacional em modelos discretos'. *CIÊNCIA E NATURA*, 42, pp. 1–13.
- Sattenspiel, L. and Dietz, K. (1995) 'A structured epidemic model incorporating geographic mobility among regions.' *Mathematical biosciences*, 128(1-2), pp. 71–91.
- da Silva, M.I., Marques, J.C., Conza, A.O., De Cezaro, A. and Gomes, A.C.F.N. (2023.No Prelo) 'The stiffness phenomena for the epidemiological sir model: a numerical approach'. In: *Latin-American Journal of Computing*.
- van den Driessche, P. and Watmough, J. (2002) 'Reproduction numbers and sub-threshold endemic equilibria for compartmental models of disease transmission'. *Mathematical Biosciences*, 180(1), pp. 29–48.



**Recommended Citation:** Chaves Marques, J *et al.* (2023). 'Some effects of population interaction on a multi-population SIRC epidemiological model'. *Rev. model. mat. sist. biol.* 3(E), e23E01, doi:10.58560/rmmsb.v03.n02.023.01



This open access article is licensed under a Creative Commons Attribution International (CC BY 4.0) <http://creativecommons.org/licenses/by/4.0/>.  
Support: